

New method for determining the bending modulus of solid and hollow fibers from
deflection tests

Vas L. M., Kling S., Czigány T., Czél G.

Accepted for publication in Textile Research Journal

Published in 2017

DOI: [10.1177/0040517516632476](https://doi.org/10.1177/0040517516632476)

New method for determining the bending modulus of solid and hollow fibers from deflection tests

László M Vas¹, Sándor Kling¹, Tibor Czigány^{1,2} and Gergely Czél²

Abstract

Bending moduli of solid and hollow glass fibres were determined by means of fibre deflection tests. The test method was modified by measuring both the vertical and horizontal displacements of the end of the deflected fibre without increasing the number of tested fibres in order to reduce the high scatter of the conventional test results obtained by measuring only the vertical displacement. Upper and lower boundary curves of the fibre end displacements were determined to filter out the inaccurate measurements e.g. when the neutral line of the fibre is not a plane but a spatial curve. Mean and coefficient of variation of the fibre bending modulus were estimated from the recorded coordinates of the fibre ends applying two newly developed statistical evaluation methods based on the individual coordinates or on their average. After comparing several evaluation methods it was demonstrated that the individual coordinate based method provided the least relative error of the average.

Keywords: glass fibre; deflection test; hollow fibre; bending modulus

1. Introduction

Increasing emphasis has been put recently on energy saving e.g. while travelling, transporting goods, or simply moving objects to save resources and reduce emissions [1]. Polymer matrix composite materials are suitable for energy efficient structures due to their high stiffness and strength combined with low density and their spread was steady in the recent decades [2]. Thermoset polymer composites typically consist of two constituents: fibres (e.g. glass, carbon, aramid) and matrix (e.g. epoxy, unsaturated polyester and other resins inc. bio-based ones [3]). The performance of composites can be improved either with advanced matrix materials including hybrid resins [4] or with novel fibre types. Most of the mechanical properties of well-designed composites are dominated by the fibre properties which therefore need to be determined accurately. Novel carbon nanotube based fibre materials [5] and fibre forming

techniques such as electrospinning [6]-[8] and special cross sections including hollow fibres are in focus for researchers to improve composite performance and to add various extra functions to the materials.

Hucker et al. [9] used hollow glass fibres (HGF) to improve the compression strength of composite plates. The hollow fibres have higher bending stiffness than solid ones in the case of same linear density, which may be exploited similarly to the high area moment of inertia of sandwich structures. Hucker et al. fabricated HGFs with various diameters, and characterised them with the fibre hollow fraction K^2 defined as the ratio of the inner d_i and outer d_o diameter of the fibres as in Equation (1).

$$0 \leq K^2 = \left(\frac{d_i}{d_o} \right)^2 < 1 \quad (1)$$

Various UD composite specimens were tested in compression and it was highlighted that the elastic modulus of the composite decreased if the hollow fraction of the fibres was increased. A 10% increase in compressive strength was achieved with $K^2 \approx 0.22$. If the elastic modulus of the fibres had been measured e.g. by fibre deflection tests, the compressive response of the plates could have been estimated and analysed. Boniface et al. [10] reported that composite plates made of hollow fibres had beneficial energy absorption properties. Hucker et al. [11] fabricated their hollow fibres from glass tubes. The pre-form was heated up and stretched to low diameter hollow fibres which were tensile tested. Low fibre wall thickness and high stretching improved the modulus and strength of the fibres.

Rosen et al. [12] investigated solid and hollow glass fibres and their composites and highlighted that the hollow glass fibre reinforced plastics (HGFRP) have better stiffness and compressive strength than those reinforced by solid fibres.

Bayat and Aghdam [13] highlighted through finite element (FE) analysis that hollow fibres had better cooling conditions during manufacture than solid ones and therefore the detrimental residual stress in the fibre due to fast cooling was reduced. Another FE study indicated that the energy absorbing capacity of the composites can be increased with increased fibre hollow fractions. Besides their beneficial mechanical properties, hollow fibres can store healing or damage indicating fluids [14] alternatively to microcapsules [15].

Mechanical properties of fibres e.g. for composite reinforcements play a key role in most applications therefore fibre testing is crucial. ASTM standards D1388 and D5732 (discontinued in 2008) propose bending stiffness measurement methods for textile samples by means of cantilever bending (Option A of ASTM D1388 and ASTM D5732) and loop

bending (Option B of ASTM D1388). Although these standard test methods apply to textile stripes, their principles are applicable to single fibres as well. The flexibility of single fibres can be measured by bending the fibre into a loop, where the smallest radius of curvature is measured before fracture of the fibre. A significant difficulty of this test method is the measurement of the curvature just before fracture [16], which may be done by post-processing a recorded video of the test. Another method utilises a cone to measure the curvature of the fibre loop at break. Tows of fibres are tensile tested in the textile industry with a knot to explore their flexibility. This test can be done on individual fibres as well. There is also a fibre test where two linked U shaped loops are bonded to paper tabs and pulled until fracture. The bending modulus of individual fibres can be determined from their deflection due to their own weight with a test similar to the cantilever test (option A of ASTM D1388 and ISO 4604:2011) as shown on Figure 1. A fibre clamped horizontally at one end exhibits a deformed shape due to its own weight, and the vertical displacement ($f_B = -y_B$) of the other end can be recorded using a scale [17],[18]. The test methods based on deflection due to own weight can be divided into two categories: where a) the vertical displacement of the end of a given length (l_0) fibre is recorded or b) the specimen length corresponding to a given chord angle (β) is recorded. Figure 1 shows the schematic of the fibre deflection test. Method a) has various evaluation processes, while method b) which is suitable for testing fabrics, cloths, and films, as well as fibres [19],[20] is usually executed using a Flexometer (ASTM D1388, D5732 and ISO 4604:2011). The horizontal displacement of the fibre end ($\Delta x_B = l_0 - x_B$) is not used for evaluation of the deflection tests so far in the literature although it could improve the accuracy of the results.

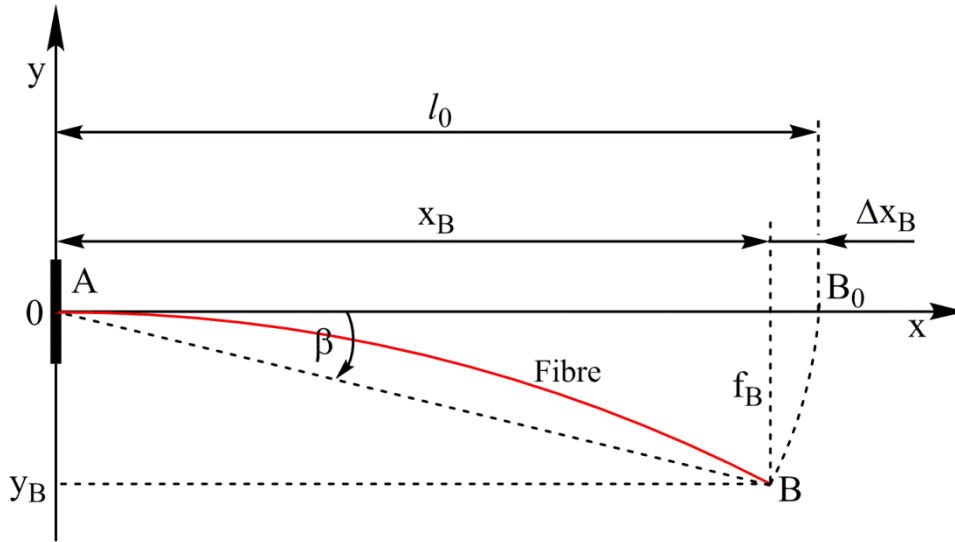


Figure 1 Geometrical schematic of the fibre deflection test ($f_B = -y_B$ and Δx_B respectively are the vertical and horizontal displacements of the fibre end)

The aim of this paper was to improve the accuracy of the fibre deflection test method by better exploitation of the test data without increasing the number of samples. The improved evaluation of the test method can result in reduced variability and better bending property estimation of the composites made of the tested fibres.

2. Materials and methods

The applied hollow fibres were supplied by R&G Faserverbundwerkstoffe GmbH (Germany) in the form of 216 g/m² areal mass woven fabric by twill weave. The solid fibres were manufactured by 3B (Belgium), in the form of continuous tows. The compositions of the two glass fibre types are similar according to inductively coupled plasma optical emission spectrometry investigations. Fibre types of similar outer diameters were selected for the experiments.

Before the deflection test the geometrical properties such as outer and inner diameters were measured on each individual fibre optically. The measured diameter data (mean and standard deviation) for hollow fibres were $d_{\text{outer}} = 13.41 \pm 1.32 \mu\text{m}$ and $d_{\text{inner}} = 6.10 \pm 1.21 \mu\text{m}$ ($K^2 = 0.21$) while that for solid fibres was $d = 13.77 \pm 0.73 \mu\text{m}$. Fibre deflection tests were performed on solid and hollow glass fibres of 50 mm length earlier and evaluated using only the vertical displacements of the fibre ends. Results of these tests were reported earlier in [18], [21] and [23]. The essence of this method is that a fibre is clamped horizontally at one end (Figure 1) and a vertical measuring scale is used to read the vertical displacement ($f_B = -y_B$) of the free

fibre end with 0.5 mm precision. More accurate results can be obtained if the horizontal displacement (Δx_B) of the fibre end is measured by another scale as well. In order to demonstrate the applicability of this latter evaluation method, further deflection tests were performed on 10 solid and 10 hollow glass fibres.

3. Results and discussion

3.1. Previous results of vertical deflection measurements

Determination of the Young's modulus through tensile testing of high performance fibres such as glass, basalt, carbon or ceramic fibres may be difficult due to gripping problems (bending fragility, compression fragility of hollow fibres, obliquity, crimp, slippage from the grips). These may result in defective specimens and various systematic and statistical errors mainly compromising the accuracy of the elongation values essential for calculating the modulus. Fibre deflection tests were performed on 50 mm long fibres in [18], [23] and evaluated using only the vertical displacements of the fibres according to the calculation method published by Holden [22]. The results including the vertical displacement (y_b) and the bending modulus (E) are visible in Table 1 [18], [23].

Fibre	Number of tested samples	Fibre end vertical displacement (y_b)				Bending modulus (E)			
		Mean [mm]	SD [mm]	CV [%]	MRE [%]	Mean [GPa]	SD [GPa]	CV [%]	MRE [%]
Solid	60	23.21	5.49	24	6	74.48	26.34	35	9
Hollow	100	17.08	6.10	36	7	98.99	55.72	56	11

Table 1 Fibre deflection test results of solid and hollow glass fibres [18],[23] (SD, CV and MRE are the standard deviation, the coefficient of variation, and the relative error of the mean respectively.)

The deflection tests of hollow fibres provided significantly higher values of mean modulus and coefficient of variation than those of the solid fibres. Some of the possible reasons for deviations and high scatter are inaccuracies of the measurement method, in diameter measurements, or in recording only the vertical displacements of the fibres. Another reason for the high scatter and the deviation in the mean values is the possible eccentricity of the hollow fibres which can result in the neutral axis of a deflected fibre not forming a plane curve as it is assumed for the evaluation. The out of test plane distance of the end point of

such an eccentric fibre can reduce its apparent vertical displacement, consequently increase the apparent elastic modulus calculated from the measurements. In order to eliminate the above mentioned problems, both the fibre deflection test method and the evaluation process were improved to enable more accurate determination of the fibre modulus based on the classical bending theory and measured values of both the vertical and horizontal displacements of the fibre end.

3.2. Calculation of large fibre deflections

The following conditions were assumed: the fibre is flexible (i.e. has a finite bending stiffness), has a circular cross section, the fibre diameter, d , is constant and small, the elongation of the fibre is negligible compared to its bending deflection and the effect of shear force is negligible. The material of the fibre is linearly elastic, and the equations of the classic bending theory can be applied (e.g. the deflected shape of the fibre is a plane curve and its cross sections remain planar).

The deflection of the fibre due to its own weight is increasing if the free length of the fibre is increased, but the change in fibre length due to deflection is negligible. Therefore the arc length between two points of the deformed shape Δs always equals the original distance Δx_0 of the same points. According to the above assumptions, $s=x_0$ during the calculation of bending moment along the fibre. Parameters of the deflected fibre shape and the schematic of the forces acting on an arc element are summarised in Figure 2.

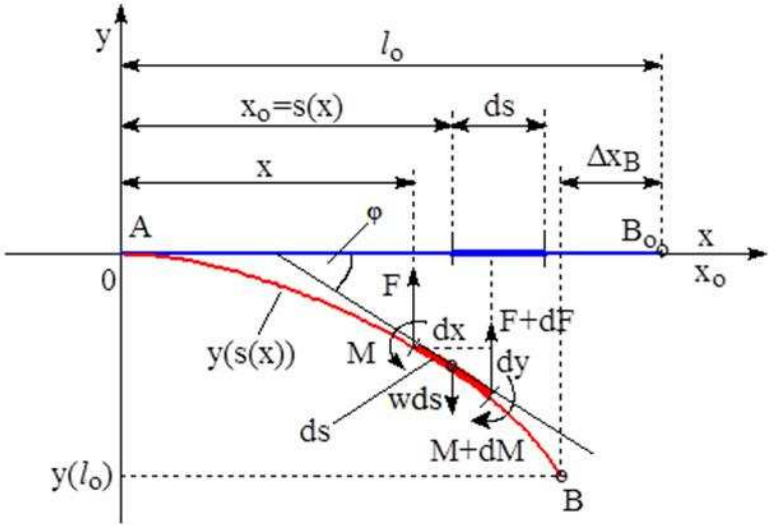


Figure 2 Schematic of the forces acting on an arc element of the deflected fibre ($y_B=y(l_0)$)

The fixed length deflected shape of the fibre is most practical to describe along its length as a function of the arc length (distance along the fibre) s and the angle φ of the tangent at any point where $x(s)$ and $y(s)$ are the coordinates of a given point and w [N/mm] is the distributed load that is the specific fibre weight. The moment $M(s)$ on an arc element can be estimated with lower and upper bounds according to Equation (2) based on inequality (3).

$$M(0) + \int_0^s F(s) \left(1 - \frac{\varphi^2(s)}{2}\right) ds \leq M(s) = M(0) + \int_0^s F(s) \cos \varphi(s) ds \leq M(0) + \int_0^s F(s) ds \quad (2)$$

$$0 < 1 - \frac{\varphi^2(s)}{2} \leq \cos \varphi(s) \leq 1 \quad (3)$$

According to the basic assumptions detailed earlier, the classic bending theory is applied as in Equation (4):

$$M = EI \frac{1}{R} = EI\kappa \quad (4)$$

Where I is the second moment of inertia of the fibre cross section, which gives the bending stiffness IE together with the bending modulus E of the fibre, R is the radius of curvature, and $\kappa=1/R=d\varphi/ds$ is the curvature. Equation (4) can be written in an integro-differential equation form, which yields Equation (5) after differentiation.

$$\frac{d^2\varphi}{ds^2} = \frac{F(s)}{EI} \cos \varphi(s) = \frac{w}{EI} (l_0 - s) \cos \varphi(s) \quad (5)$$

The second order non-linear differential Equation (5) cannot be solved analytically, therefore upper and lower bounds are determined first using inequality (2) and then numerical methods are applied for a more accurate solution.

3.3. Boundary curves of the fibre end positions

The upper bound of $\cos \varphi(s) \leq 1$, part of inequality (3) is given first in Equation (6):

$$\frac{d^2\varphi}{ds^2} = \frac{F(s)}{EI} \cos \varphi(s) = \frac{w}{EI} (l_0 - s) \cos \varphi(s) \leq \frac{w}{EI} (l_0 - s) \quad (6)$$

Therefore the differential inequality can be written as in Equation (7)

$$\frac{d^2\varphi}{ds^2} \leq \frac{w}{EI} (l_0 - s) \quad (7)$$

Integration of Equation (7) yields:

$$\kappa(s) = \frac{d\varphi}{ds} = C_1 + \frac{w}{EI} \left(l_0 s - \frac{s^2}{2} \right) = C_1 + \frac{wl_0^2}{2EI} \left(2 \frac{s}{l_0} - \frac{s^2}{l_0^2} \right) \quad (8)$$

Integration constant C_1 can be determined if we consider that the curvature is zero at the free end of the fibre at $s=l_0$ as given in Equation (9):

$$\kappa(l_0) = C_1 + \frac{wl_0^2}{2EI} = 0 \Rightarrow C_1 = -\frac{wl_0^2}{2EI} \quad (9)$$

Equation (8) gives a negative curvature for the deflected fibre shape if C_1 is substituted according to (10), which agrees with Figure 3.

$$\kappa(s) = \frac{d\varphi}{ds} = -\frac{wl_0^2}{2EI} \left(1 - \frac{s}{l_0} \right)^2 \quad (10)$$

Equation (10) indicates that the essence of the upper boundary estimation is that $x_0=s$ is also considered when calculating the moments. Moments, higher than the actual ones are therefore used which results in over-estimated absolute curvature values. In the case of $\cos\varphi=1$ the expression of the elementary lever-arm in Equation (2) changes from $\cos\varphi ds$ into ds hence this simplification results in a kind of uniformly distributed force system, where the forces acting on the arc elements point to the direction of the centre of curvature instead of being vertical.

Equation (10) can be integrated, considering $\varphi(0)=0$ to obtain the tangent angle of the estimated fibre shape. The arranged form of Equation (11) shows that the angle of the tangent is always negative along the fibre ($0 \leq s \leq l_0$) which agrees with Figure 2.

$$\varphi(s) = -\Omega \left(1 - \left(1 - \frac{s}{l_0} \right)^3 \right), \quad \Omega = \frac{wl_0^3}{6EI} \quad (11)$$

The fibre length dependent Ω constant is one sixth of Holden's k constant. The parametric equations of the fibre shape with $0 \leq t=s/l_0 \leq 1$ can be calculated using $\varphi(s)$ as given in (12).

$$\begin{aligned} y(s) &= \int_0^s \sin \varphi(s) ds = -l_0 \int_0^{s/l_0} \sin \Omega \left(1 - (1-t)^3 \right) dt \\ x(s) &= \int_0^s \cos \varphi(s) ds = l_0 \int_0^{s/l_0} \cos \Omega \left(1 - (1-t)^3 \right) dt \end{aligned} \quad (12)$$

The lower boundary curve of the fibre deflection can be generated, if the curvature of the fibre is assumed to be zero all along its length i.e. the fibre remains straight and the fibre is rotated

around the fixed end which is transformed into a hinge. Consequently, the curve of fibre end-point is a circular arc described by Equation (13):

$$\frac{y(l_0)}{l_0} = -\sqrt{1 - \left(\frac{x(l_0)}{l_0}\right)^2} \quad (13)$$

where the end-point coordinates are $x_B = x(l_0)$ and $y_B = y(l_0)$ as indicated in Figures 1 and 2.

All the experimental data points of the solid fibres fall between the boundary curves, but four of those of the hollow fibres (including two overlapping ones) falls outside the boundary for maximum curvature, probably due to measuring artefacts. These are excluded with the aid of the boundary curves to increase the accuracy of the remaining data points. A significant scatter is identified in the test data, therefore the accurate solution between the boundary curves is yet to be found for the correct determination of the average elastic modulus of the fibres.

3.4. Exact solution using the fourth-order Runge-Kutta method

The so-called fourth-order Runge-Kutta method [24] is an effective numerical tool for solving ordinary differential equations. It provides explicit solution applying recursive formulae for calculating the next value of ordinate from the weighted sum of four former ones and a finite abscissa increase. It is primarily used for first order differential equations and initial value problems, but it can be applied successfully to solve boundary value problems of higher order equations by using the so called shooting method based on iterations [24]. As the fourth-order Runge-Kutta method provides fourth-order accuracy (fifth-order error) the same fifth-order error definition was applied in calculations performed with Microsoft Excel. The normalised arc length interval of [0,1] was divided into 100 equal sections and the calculations were executed with a step size of $\Delta t = 0.01$. Figure 3 shows the calculated coordinates of the fibre end-point as a function of parameter Ω . These curves correspond to those calculated by Holden [22].

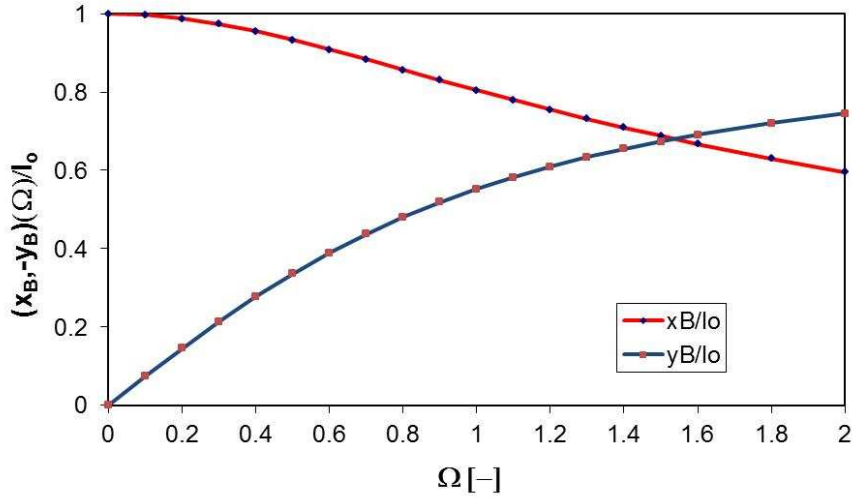


Figure 3 Normalised coordinates of the fibre end as a function of parameter Ω

3.5. New evaluation method and test results

The curves of Figure 3 can be considered as parametrised inverse functions from the test evaluation point of view since the measured values are the $(\Delta x_B = l_0 - x_B, f_B = -y_B)$ displacement components of the fibre end-point and Ω is the parameter to be determined. The polynomial trends of the normally measured y and the previously not exploited x normalised coordinates of the fibre end-point were used to determine the Ω parameter explicitly with high coefficient of determination ($R^2 \geq 0.9998$). Equations (14) and (15) can directly be used for test evaluation determining Ω from the measured coordinates of the fibre end ($y_B < 0, f_B = -y_B$ in Figures 1 and 2).

$$\Omega_x = 11.351 \frac{y_B(\Omega)}{l_0}^4 - 10.75 \frac{y_B(\Omega)}{l_0}^3 + 4.0149 \frac{y_B(\Omega)}{l_0}^2 + 0.943 \frac{y_B(\Omega)}{l_0} \quad (14)$$

$$\Omega_y = 10.049 \sqrt{1 - \frac{x_B(\Omega)}{l_0}}^4 - 6.0174 \sqrt{1 - \frac{x_B(\Omega)}{l_0}}^3 + 2.1654 \sqrt{1 - \frac{x_B(\Omega)}{l_0}}^2 + 1.6091 \sqrt{1 - \frac{x_B(\Omega)}{l_0}} \quad (15)$$

In case of a Flexometer, the l_0 fibre length belonging to a given β angle of the fibre chord (Figure 1) is measured and the parameter Ω containing l_0 according to Equation (11) can be estimated with a second order polynomial as a function of $\tan \beta = -y_B/x_B$ with a good agreement ($R^2 \approx 1$) as follows.

$$\Omega_{y/x} = 0.2446(\tan \beta)^2 + 1.2919 \tan \beta \quad (16)$$

Figure 4 shows the measured coordinates of the fibre end-point, the boundary curves according to Equations (12) and (13) as well as the fibre-end curve determined with the fourth-order Runge-Kutta method that runs in the middle of the area between the boundary curves.

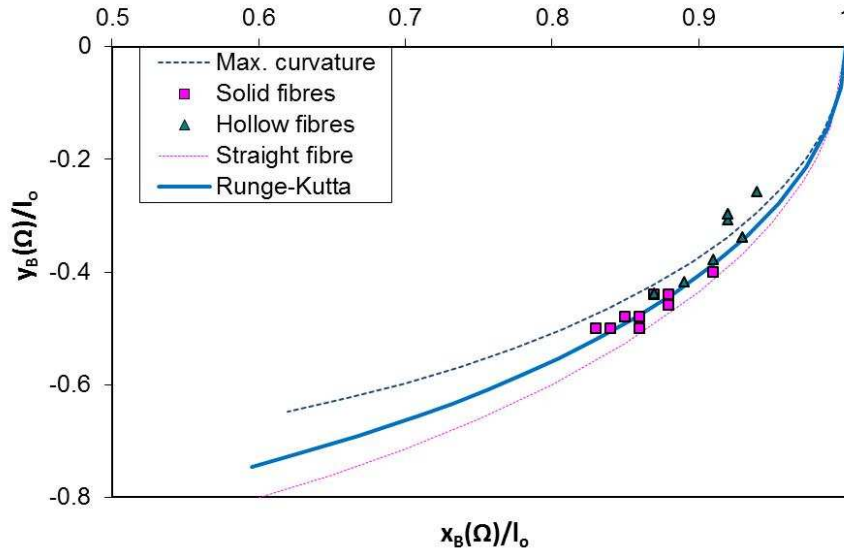


Figure 4 Measured coordinates of fibre end-points, boundary curves, and the fibre-end curve determined with the Runge-Kutta method

The end-point curve generated by using the Runge-Kutta method, can be described with a simple second order polynomial with excellent fit ($R^2=0.9999$) where the independent variable is a square root type expression given by:

$$\frac{-y_B(\Omega)}{l_0} = -0.3369 \left(\sqrt{1 - \frac{x_B(\Omega)}{l_0}} \right)^2 + 1.3939 \sqrt{1 - \frac{x_B(\Omega)}{l_0}} \quad (17)$$

Figure 5 shows this simple description graphically, where the measured positions of the fibre end-points are also marked.

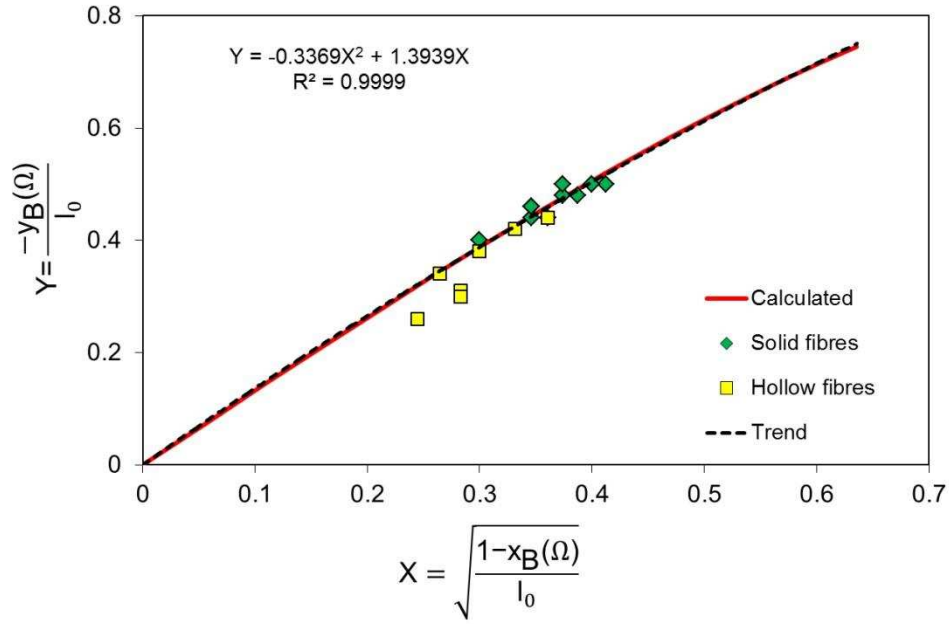


Figure 5 Fibre end-point curve after transforming the independent variable

As usual in the literature measuring a single value such as coordinate y or x or angle β the parameter Ω can be calculated with Equation (14) or (15) or (16), respectively, while measuring e.g. end-point coordinates y_B and x_B simultaneously provides two estimations for Ω by using Equations (14) and (15). These two latter differ because of errors in the measurements (in the fibre length, end-point position, fibre diameter and roundness) and possible material in-homogeneities (in e.g. elastic modulus or density). Hence due to measuring errors and in-homogeneities the measured points scatter around the theoretical end-point curve (points marked with ‘*’ in Figure 6) or moreover they may gather around deviated curves above or below the right curve (points marked by ‘x’ or ‘o’ in Figure 6). The possible positions of the measured end-point sets are depicted in Figure 6. It is also true for the average points of these possible end-point sets (marked by red and blue ‘O’ in Figure 6) that are determined by the mean values of the measured end-point coordinates. (For the sake of simpler illustration in Figure 6 the intersection points of the coordinate lines of the red and blue average points are equal to those created by these coordinate lines and the theoretical end-point curve)

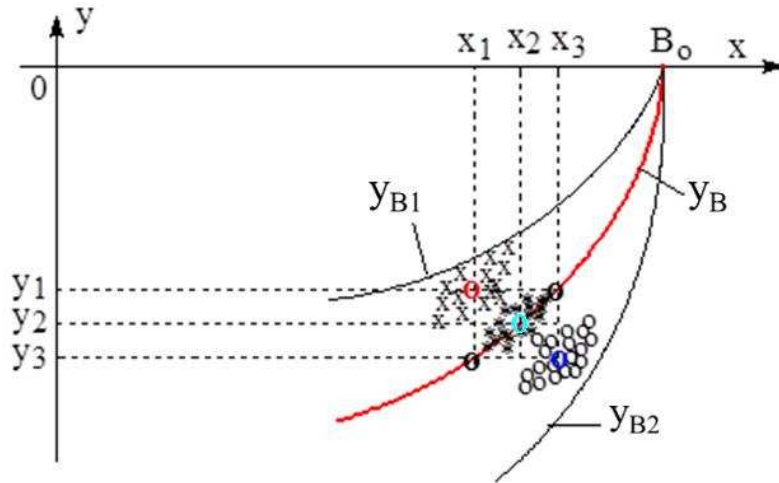


Figure 6 Three possible positions of the measured end-point sets (x , $*$, o) and their average points (red, cyan, and blue \bullet) and intersection points (black \bullet) of the theoretical end-point curve and the coordinate lines of average points red and blue

The estimated values of the Ω parameter from both coordinates are consistent with each other only if the measured points scatter along the correct curve. If the end-points evaluated from x and y coordinates aggregate around separate points away from the correct curve, they yield different Ω for x and y coordinates. Therefore it is worth considering an averaging based evaluation method which exploits both coordinates of each fibre end-point (unlike conventional approaches using only one coordinate). Two suitable methods can be proposed: the method of average points and the method of individual coordinates.

3.6. Average point method

If the average point determined by the measured coordinates x and y does not fall onto the correct curve the best estimation can be obtained by normal projection of the experimental average point onto the correct curve calculated by the Runge-Kutta method. Such a point can be obtained as follows. Intersecting the correct curve with the coordinate lines running through the average point separately gives two intersection points on the correct curve as shown on Figure 6 (black ' \bullet '-s). The midpoint of the chord between the intersection points, that can be obtained as an average provides a good estimation for the right projected point on the correct curve (cyan ' \bullet '). The corresponding parameter Ω can be determined by calculating the Ω values directly from the intersection points separately for the coordinates y and x (Ω_y and Ω_x) using Equations (14) and (15) and their average is then computed with Equation (18).

$$\bar{\Omega} := \frac{1}{2}(\bar{\Omega}_x + \bar{\Omega}_y) = \frac{1}{2n} \left(\sum_{i=1}^n \Omega_{x,i} + \sum_{i=1}^n \Omega_{y,i} \right) \quad (18)$$

The tensile elastic modulus (E) of the fibre can be obtained from Equation (19).

$$E = \frac{wl_o^3}{\bar{\Omega}} = \frac{C_E}{\bar{\Omega}} \quad (19)$$

where the constant, C_E , is defined by Equation (19) and determined by the fibre geometry and material. For a hollow fibre with outer and inner diameters d_o and d_i , and the cross-sectional areas calculated with them $A_o = d_o^2 \pi/4$ and $A_i = d_i^2 \pi/4$ respectively, the terms including cross-sectional geometric parameters can be formulated as in Equation (20).

$$\frac{w}{I} = \frac{A \rho g}{\frac{d_o^4 \pi}{64} \frac{d_i^4 \pi}{64}} = \frac{A \rho g}{\frac{A}{4\pi} \frac{A_o}{A_o} \left(1 + \frac{d_i^2}{d_o^2}\right)} = 4\pi g \frac{\rho}{A_o} \phi_d \quad (20a)$$

$$\frac{1}{2} < \phi_d = \frac{1}{1 + \frac{d_i^2}{d_o^2}} = \frac{1}{1 + K^2} \leq 1 \quad (20b)$$

Where $A = A_o - A_i$ is the cross-sectional area of the hollow fibre, while $d_i = 0$ and $\phi_d = 1$ are true for solid fibres.

The average point method can be applied effectively to determine the average modulus of the fibres if the fibre geometry is consistent or its parameters are of small standard deviations hence C_E can be assumed constant. Otherwise assessing the error of the modulus is problematic due to non-linearity in the formulations.

3.7. Individual coordinates method

This case the coordinates of each measured end-point (P_i) are handled separately. $\Omega_{x,i}$ and $\Omega_{y,i}$ determined for the x_i and y_i coordinates of each P_i are not averaged, but the individual $E_{x,i}$ és $E_{y,i}$ values are calculated with the corresponding C_{Ei} and averaged according to Equation (21).

$$\bar{E} := \frac{1}{2}(\bar{E}_x + \bar{E}_y) = \frac{1}{2n} \left(\sum_{i=1}^n E_{x,i} + \sum_{i=1}^n E_{y,i} \right) = \frac{1}{2n} \sum_{i=1}^n C_{Ei} \left(\frac{1}{\Omega_{x,i}} + \frac{1}{\Omega_{y,i}} \right) \quad (20)$$

Alternative to the average point method, the reciprocals of the Ω parameters calculated from the individual coordinates of the end-points are averaged here. The error of \bar{E} average values

can be estimated with the experimental standard deviation S_E of the individual values. It is assumed that the error of the individually measured x and y end-point coordinates are independent, thus the 95% confidence intervals and the δ_E relative errors can be written as in Equation (22):

$$E \approx \bar{E} \pm t_{n,95\%} \frac{S_E}{\sqrt{n}} = \bar{E} \left(1 \pm t_{n,95\%} \frac{S_E / \bar{E}}{\sqrt{n}} \right) = \bar{E} (1 \pm \delta_E) \quad (21)$$

Where S_E is the standard deviation of the individual E values and $t_{n,95\%}$ is the relevant critical value of the Student distribution [25] .

3.8. Demonstration of applicability

Tables 2 and 3 present the bending modulus values (E) calculated with different approaches from Ω_x , Ω_y , Ω_A and $\Omega_{Y/X}$ based on the results of 10 deflection measurements carried out on solid and hollow glass fibres. The tables contain the average (Mean) bending modulus (E) calculated with equation (21), the coefficient of variation (CV) and the relative error of the mean value (MRE; 10 data: $t_{n,95\%}=2.262$). The Ω_A parameter of a fibre was calculated as the average of the individual values Ω_x and Ω_y with Equations (15) and (14), while $\Omega_{Y/X}$ was determined with Equation (16).

The following observations can be made analysing the data in the tables:

- (i) the difference between the Ω_x and Ω_y based mean E values (10 data) is minor (<0.15%) for the solid fibres, but in case of the hollow fibres the difference is much higher (~6%)
- (ii) the CV of the bending modulus for the hollow fibres (8.4-11.1%) is higher than that of the solid fibres (7.3-7.8%);
- (iii) the individual coordinate method (20 data; $t_{n,95\%}=2.093$) is the most advantageous, which gives the lowest relative error of the mean value (MRE) for both the solid (1.7%) and the hollow (2.2%) fibres.

Method of calculation	Bending stiffness (IE)	Bending modulus (E) (10 data)			Bending modulus (E) (20 data)		
	Mean [N·mm ²]	Mean [GPa]	CV [%]	MRE [%]	Mean [GPa]	CV [%]	MRE [%]
Ω_y	1.03E-04	69.0	7.8	2.48	68.9	7.5	1.7
Ω_x	1.03E-04	68.9	7.3	2.30			
Ω_A	1.03E-04	69.0	8.7	2.75			
$\Omega_{Y/X}$	1.03E-04	68.5	7.8	2.47			

Table 2 Calculated parameters for solid fibres

Method of calculation	Bending stiffness (IE)	Bending modulus (E) (10 data)			Bending modulus (E) (20 data)		
	Mean [N·mm ²]	Mean [GPa]	CV [%]	MRE [%]	Mean [GPa]	CV [%]	MRE [%]
Ω_Y	1.10E-04	69.5	8.4	2.64	71.6	9.7	2.2
Ω_X	1.17E-04	73.6	11.1	3.51			
Ω_A	1.04E-04	66.1	6.9	2.18			
$\Omega_{Y/X}$	1.17E-04	73.6	11.0	3.47			

Table 3 Calculated parameters for hollow fibres before discarding the outlier data points

High scatter is attributed mainly to the four data points lying out of the boundary curves in case of the hollow fibres. Discarding these four outliers the remaining points fit very well to the end-point curve (Figure 4). As a consequence the CV decreased from 9.7% to 7.2% (20 and 12 data) while the relative error of the average modulus (MRE; 6 data: $t_{n,95\%}=2.571$; 12 data: $t_{n,95\%}=2.201$) increased from 2.2% to 4.6% as it can be seen in Table 4. The increase in MRE despite of the reduction in CV issued from the decrease in the number of data (20→16) and the mean (71.6 GPa→66.2 GPa). The latter was due to the effect that the outliers belonged to apparently stiffer fibres with smaller vertical displacement. This error was probably caused by out of the plane displacements of the fibre end-points (see Figure 4).

Method of calculation	Bending stiffness (IE)	Bending modulus (E) (6 data)			Bending modulus (E) (12 data)		
	Mean [N·mm ²]	Mean [GPa]	CV [%]	MRE [%]	Mean [GPa]	CV [%]	MRE [%]
Ω_Y	9.09E-05	67.1	7.4	7.72	66.2	7.2	4.6
Ω_X	8.90E-05	65.2	7.3	7.70			
Ω_A	8.99E-05	66.1	7.2	7.57			
$\Omega_{Y/X}$	9.13E-05	67.1	7.0	7.33			

Table 4 Calculated parameters for hollow fibres after discarding the outlier data points

By measuring both the vertical and the horizontal coordinates of the fibre end-point and using the individual coordinate method for evaluation the MRE of the elastic modulus was reduced to 69% or 83% of the original values for the solid and hollow fibres, respectively. In addition, discarding the outliers by using the determined boundary curves reduced the number of valuable data points for hollow fibres however decreased the CV as well. In the case of much more test data the filtering can also be advantageous for the MRE.

4. Conclusion

The elastic modulus of solid and hollow fibres was determined from fibre deflection tests. Our previous work highlighted that taking only the vertical displacement of the fibre end-point into account results in excessive error and high scatter. In order to reduce the errors, the horizontal displacement was measured as well. The theoretical curve of the fibre end-point was determined with the Runge-Kutta method as well as upper and lower boundary curves were found which allowed the identification and filtering of the outliers that were obviously erroneous data points. For making the best use of the test data two statistical evaluation methods were developed. In order to demonstrate the applicability of the methods developed, some fibre deflection tests were performed on solid and hollow glass fibres. The evaluation using the individual coordinate method resulted in 17-31% reduction in the relative error of the determined mean elastic modulus of solid and hollow fibres. Discarding 4 outlier data-points by using the boundary curves provided 26% reduction in CV for the hollow fibres. Consequently, the new method can improve the accuracy of the modulus evaluation without increasing the number of tested fibres therefore it provides more accurate input for analysis of the stiffness of composite structures than the conventional method using only the vertical displacement of the fibre end-point. Future task can be the extensive validation of the new evaluation method on various fibre types.

Acknowledgement

This work was connected to the scientific program of the "Development of quality-oriented and harmonized R+D+I strategy and functional model at BME" project and performed within the framework of the project "Talent care and cultivation in the scientific workshops of BME" project. This project was supported by the New Széchenyi Plan (Project ID: TÁMOP-4.2.1/B-09/1/KMR-2010-0002) and by grant TÁMOP - 4.2.2.B-10/1--2010-0009. This work was supported by Hungarian Scientific Research Fund (OTKA K 116070). Czigány acknowledges a Charles Simonyi scholarship. S. Kling would like to give thanks to the Pro Progressio Foundation for the subsidy provided for the research. G. Czél acknowledges the Hungarian Academy of Sciences for funding through the Post-Doctoral Researcher Programme fellowship scheme and the János Bolyai scholarship.

References

- [1] Mc Lean-Conner P. Energy efficiency: Principles and practices. Tusla: PennWell, 2009.
- [2] Song K, Zhang Y, Meng J, Green EC, Tajaddod N, Li H, and Minus ML. Structural polymer-based carbon nanotube composite fibers: Understanding the processing–structure–performance relationship. *Materials* 2013; 6: 2543-2577.
- [3] Belcher LK, Drzal LT, Misra M, and Mohanty AK. Physico-mechanical and morphological studies of bio-fiber reinforced bio-based epoxy resin composites for automotive exterior applications. *Polymer Materials: Science and Engineering* 2002; 87: 256-257.
- [4] Mészáros L and Turcsán T. Development and mechanical properties of carbon fibre reinforced EP/VE hybrid composite systems. *Period Polytech Mech* 2014; 58: 127-133.
- [5] Zhu C, Chen J, Koziol KK, Gilman JW, Trulove PC and Rahatekar SS. Effect of fibre spinning conditions on the electrical properties of cellulose and carbon nanotube composite fibres spun using ionic liquid as a benign solvent. *Express Polym Lett* 2014; 8: 154–163.
- [6] Molnár K, Košťáková E and Mészáros L. The effect of needleless electrospun nanofibrous interleaves on mechanical properties of carbon fabrics/epoxy laminates. *Express Polym Lett* 2014; 8: 62-72.
- [7] Kancheva M, Toncheva A, Manolova N and Rashkov I. Enhancing the mechanical properties of electrospun polyester mats by heat treatment. *Express Polym Lett* 2015; 9: 49-65.
- [8] Rakesh GR, Ranjit GS, Karthikeyan KK, Radhakrishnan P and Biji P. A facile route for controlled alignment of carbon nanotube-reinforced, electrospun nanofibers using slotted collector plates. *Express Polym Lett* 2015; 9: 105-118.
- [9] Hucker M, Bond I, Bleay S and Haq S. Experimental evaluation of unidirectional hollow glass fibre/epoxy composites under compressive loading. *Compos Part A-Appl S* 2003; 34: 927-932.
- [10] Boniface L, Foreman A and Hitchen S. Comparative evaluation of solid and hollow S2 glass fibre-epoxy laminates. *Plast Rub Compos Pro* 1998; 27: 234-239.
- [11] Hucker MJ, Bond IP, Haq S, Bleay S and Foreman A. Influence of manufacturing parameters on the tensile strengths of hollow and solid glass fibres. *J Mater Sci* 2002; 37: 309-315.
- [12] Rosen W, Ketler E and Hashin Z. Hollow glass fibre reinforced plastics. Report, General Electric Missile & Space Division, Philadelphia, USA, 1962.
- [13] Bayat M and Aghdam MM. A micromechanics based analysis of hollow fiber composites using DQEM. *Compos Part B- Eng* 2012; 43: 2921-2929.
- [14] Trask RS and Bond IP. Biomimetic self-healing of advanced composite structures using hollow glass fibres. *Smart Mater Struct* 2006; 15: 704-710.
- [15] Noh HH and Lee JK. Microencapsulation of self-healing agents containing a fluorescent dye. *Express Polym Lett* 2013; 7: 88-94.
- [16] DeTeresa SJ, Allen SR and Farris RJ. Composite applications. New York: VCH Publisher, 1992.
- [17] Siebel E. *Handbuch der Werkstoffprüfung*. Berlin: Springer, 1960.
- [18] Kling S and Czigany T. A comparative analysis of hollow and solid glass fibers. *Text Res J* 2013; 83:1764-1772.

- [19] Morton WE and Hearle JWS. Physical properties of textile fibres. Cambridge: Woodhead Publishing Limited, 2008.
- [20] Sommer H, Winkler F and Sieber E. Die Prüfung der Textilien. Berlin: Springer-Verlag, 1960.
- [21] Kling S and Czigány T. Damage detection and self-repair in hollow glass fiber fabric-reinforced epoxy composites via fiber filling. *Compos Sci Technol* 2014; 99:82-84.
- [22] Holden J. On the finite deflections of thin beams. *Int J Solids Struct* 1972; 8:1051-1055.
- [23] Kling S. Polymer composites reinforced by hollow glass fibres. PhD Thesis (in Hungarian), Budapest University of Technology and Economics, Hungary, 2014.
- [24] Spiteri RJ and Ruuth SJ. Non-linear evolution using optimal fourth-order strong-stability-preserving Runge–Kutta methods. *Math Comput Simulat* 2003; 62:125-135.
- [25] Himmelblau DM. Process Analysis by Statistical Methods. New York: John Wiley & Sons. Inc., 1970.